Iraqi Journal of Physics, 2026
https://doi.org/10.30723/ijp.v24i3.1508

Vol.24 No.3, PP.54-64
P-ISSN: 2070-4003
E-ISSN: 2664-5548

Effect of Oxidant Ratio on the Structural and Electrical Behavior of Biopolymer Electrolyte Based on Chitosan: PANI Blend

Elaaf A. Swady[1] and Mohammed K. Jawad[1*]
[1]*Department of Physics, College of Science, University of Baghdad, Baghdad, Iraq*
[*]Corresponding author: Mohammed.Jawad@sc.uobaghdad.edu.iq

Abstract

Chitosan/polyaniline (Cs/PANI) biopolymer electrolyte films were prepared by the solution casting method to investigate the influence of the oxidant-to-monomer ratio during PANI synthesis on their structural, optical, thermal, morphological, and electrical properties. Fourier transform infrared spectroscopy (FTIR) confirmed the interaction between Cs and PANI through characteristic shifts in the absorption bands, indicating enhanced intermolecular interactions. UV-vis. Analysis revealed that increasing the oxidant ratio reduced the optical band gap from 2 to 1.8 eV, while electrical measurements demonstrated an improvement in ionic conductivity from 8.47×10^{-3} to 1.06×10^{-2} S. cm^{-1}. Scanning electron microscopy (SEM) revealed a more homogeneous distribution of PANI within the Cs matrix, with reduced particle agglomeration. In contrast, differential scanning calorimetry (DSC) indicated enhanced thermal stability and improved polymer chain mobility. These results demonstrate that optimizing the oxidant ratio is an effective approach for enhancing the structural organization, charge transport, and thermal performance of Cs/PANI biopolymer electrolytes, highlighting their potential for solid-state energy storage and flexible electronic applications.

Article Info.

Keywords:
PANI, Chitosan, Oxidative Polymerization, Physical Properties, Ionic Conductivity.

Article history:
Received:Aug. 02, 2025
Revised: Nov. 30, 2025
Accepted: Dec.03, 2025
Published:Sep. 01, 2026

1. Introduction

Recently, solid blend electrolytes (SBEs) have attracted great interest, as they can be used in energy storage technologies. These materials are regarded as favorable competitors in the fabrication of advanced energy storage devices, as they have the best chemical, thermal, and mechanical properties. Moreover, they are critical for increasing ionic conductivity because they retain water effectively and can be applied to high-performance applications [1]. SBEs can improve performance through polymer blending, cross-linking enhancement, and the addition of dopants, inorganic fillers, or plasticizers, using a multiplicity of strategies. SBEs have naturally low ionic conductivity and wettability, which is inadequate in certain cases and can be improved with plasticizers or liquid solvents. Nonetheless, the addition can decrease mechanical stability and pose the same safety issues as liquid electrolytes, e.g., leakage and flammability risks [2].

Polymer blending, however, offers a promising solution, as it can combine the complementary properties of various polymers, thereby improving electrochemical and mechanical performance. They have also attracted growing interest because of their unique physicochemical and optical properties, making them a promising area of research [3]. They are the best and most practical of these methods. It is a hybrid (chemical or physical) procedure of combining two or more polymers. In general, using blended polymers is preferable to individual components, and they can be used in industrial and commercial settings as well. The approach enhances mechanical stability, ionic conductivity, and mechanical strength [4].

A widely used natural polymer, which is a derivative of chitin, is chitosan (Cs), which is a linear polysaccharide polymer that contains a large percentage of N-acetyl groups. Its structural and electrical characteristics may be readily adjusted because chitosan can be subjected to numerous physicochemical manipulations, e.g., mechanochemical treatment, plasma-induced amorphization, or copolymerization [5]. Chitosan is considered the second-most-abundant polymer after cellulose due to its optical, thermal, and mechanical properties [6]. It is an electrical insulator; its structure must be altered to increase its electrical and ionic

conductivity. It is a natural polymer that possesses very good biological properties, as it is biocompatible and biodegradable. It is soluble in dilute acids and is renewable [7].

Biopolymer electrolytes have also been gaining momentum in recent years because they have the potential to be used in biocompatible, environmentally friendly energy-storage devices. Such materials are a potential alternative to traditional electrolytes, as they do not contain toxic elements, are biodegradable, and are environmentally friendly [8]. An important point in the development of new electroactive conducting polymers is critical. Electroactive conducting polymers have received much interest over the past decades owing to their numerous potential applications. One of them is polyaniline (PANI), with its high electrical conductivity, environmental stability, low density, ease of synthesis and processing, and cost-effectiveness. It has been successfully used in battery recharging, including zinc-based and Lithium-Ion Batteries (LIBs) [9]. The reason that conductive polymers are highly researched is due to their ease of synthesis, high conductivity, chemical stability, affordability, and unusual electrochemical redox characteristics [10]. The ionic conductivity of a nonplasticized polymer electrolyte is lower when excessive salt results in the formation of ion pairs and cross-linking, which hinder the movement of the polymer chain on a segmental scale [11].

The objective of the work is to study the impact of the oxidant ratio (APS, $(NH_4)_2S_2O_8$) on the structural, optical, thermal, and electrical properties of PANI blends with chitosan, and to optimize its application as a biopolymer electrolyte for smart-material and energy-related applications.

2. Experimental Part

2.1. Materials

Chitosan (medium molecular weight, viscosity 300–1000 cps, ≥98% purity, Glentham Life Sciences, UK), aniline (≥ 99.5%, Sigma-Aldrich), and ammonium persulfate (APS, $(NH_4)_2S_2O_8$, ≥ 98%, Sigma-Aldrich) were used as received. The average molecular weight of chitosan was approximately 1,250,000 Da. All glassware and instruments were thoroughly cleaned and dried before use. PANI was synthesized via chemical oxidative polymerization of aniline monomer using oxidants like ammonium persulfate (APS, $(NH_4)_2S_2O_8$). Two batches of PANI (M1 and M2) were prepared by varying the amount of ammonium persulfate and monomer aniline, as shown in Table 1. The specified amounts of ammonium persulfate and the monomer aniline were separately dissolved in 50 mL of distilled water with constant stirring using a magnetic stirrer at 300 rpm at room temperature (25 ± 1 °C) for 2 hrs for the ammonium persulfate solution and 1 hour for the aniline solution.

The monomer solution was dropwise introduced to the oxidant solution in an ice bath (to ensure that the temperature stayed at 0-5 ^oC,) to initiate the polymerization process, with constant stirring with a magnetic stirrer. The color of the mixture changed to dark green, indicating the formation of PANI. The polymerization took about 4 hours to elute full reaction. The mixture was allowed to settle for 30 minutes, and the polymer obtained was filtered and thoroughly washed with distilled water. The PANI obtained was dried in an oven at 40 ^oC for 4 hours and subsequently ground to a fine powder. The aniline polymerization reaction had the chemical equation shown in Fig. 1.

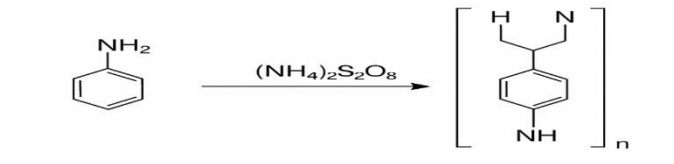

Figure 1: Polymerization reaction of PANI.

Table 1: Composition of the prepared samples (M1 and M2).

	Ammonium persulfate + distilled water	**Monomer aniline + distilled water**
M1	2.5 g + 50 mL	1 mL + 50 mL
M2	4 g + 50 mL	2 mL + 50 mL

2.2. Blend Preparation

To prepare the Cs:PANI blend, first, 1 g of chitosan was dissolved in 60 mL of 1% acetic acid (60 mL). The mixture was magnetically stirred for 5 hours to allow chitosan to fully dissolve, yielding a clear, homogeneous solution. 0.1 g of PANI (M1 and M2) was separately dissolved in 5 mL of dimethyl sulfoxide (DMSO) until complete dissolution was attained. Both PANI solutions (M1 and M2) were subsequently added dropwise to the chitosan solution under continuous stirring for 8 hours to ensure that the polymer-polymer mixture was well mixed and interacted appropriately. These blends were labelled R1 and R2, corresponding to the PANI that was prepared using M1 and M2, respectively. Table 2 summarizes the compositions of the prepared blends.

Table 2: The composition of (R1&R2) blend.

Samples	**Cs + Acetic Acid**	**PANI + DMSO**
R1	1 g + 60 mL	0.1 g M1 + 5 mL
R2	1 g + 60 mL	0.1 g M2 + 5 mL

3. Results and Discussion

3.1. FTIR Results

The FTIR analysis was used in the study of the intermolecular interactions between Cs and PANI in the prepared Cs:PANI blends (R1 and R2). The obtained FTIR spectra are depicted in Fig. 2, with the key absorption bands and their assignments listed in Table 3. Both spectra showed typical absorption peaks related to the Cs molecular backbone, besides a few other bands related to PANI. The extensive absorption band at about 3400 cm^{-1} in the two samples was attributed to the OH stretching bands of the hydroxyl group of chitosan. This peak was wider and slightly displaced in sample R2, indicating a higher degree of hydrogen bonding and greater molecular organization. Both spectra also showed a CH or C-H stretching region at 2800-3000 cm^{-1}, which is an aliphatic vibration of the polymer chains [12].

A number of variations in the amide and fingerprint area between R1 and R2 were noted. For R1, the amide I peak at 1654.96 shifted to 1642.65 cm^{-1} in R2, indicating modification to the environment of the amide and hydrogen bonding. On the same note, the bending vibration of NH_2 of R1 moved to 1568.83 and to 1573.75 cm^{-1} for R2, which means that interactions between chains in the latter are stronger. Both R1 and R2 showed CH_2 bending modes at 1408.89 and 1413.81 cm^{-1}, respectively, with slight structural conformation variation.

Amide III, associated with amide III vibrations, was at 1312.92 and 1317.84 cm^{-1} for R1 and R2, respectively, proving a more compact and ordered polymeric network in R2. The C=O stretch peak resonance was fixed at 1150.51 cm^{-1}. The C-O-C peak was at 953.66 cm^{-1} in both samples, indicating the presence of ether links [13]. Minor changes were noted in the lower-frequency region: the 705.13 cm^{-1} band in R1 changed to 707.59 cm^{-1} in R2, and the C-H bending vibration marginally shifted between 616.54 cm^{-1} (R1) and 614.08 cm^{-1} (R2). The

peak at 486.12 cm^{-1} for R1 appeared at 513.19 cm^{-1} for R2, indicating slight structural rearrangements and stronger molecular interactions in the R2 blend [14]. In general, the recorded changes in FTIR peaks (especially in amide I and NH2 peaks) indicate increased strength of hydrogen bonding and larger-scale arrangement of the molecules in R2, which directly accounts for the high ionic conductivity.

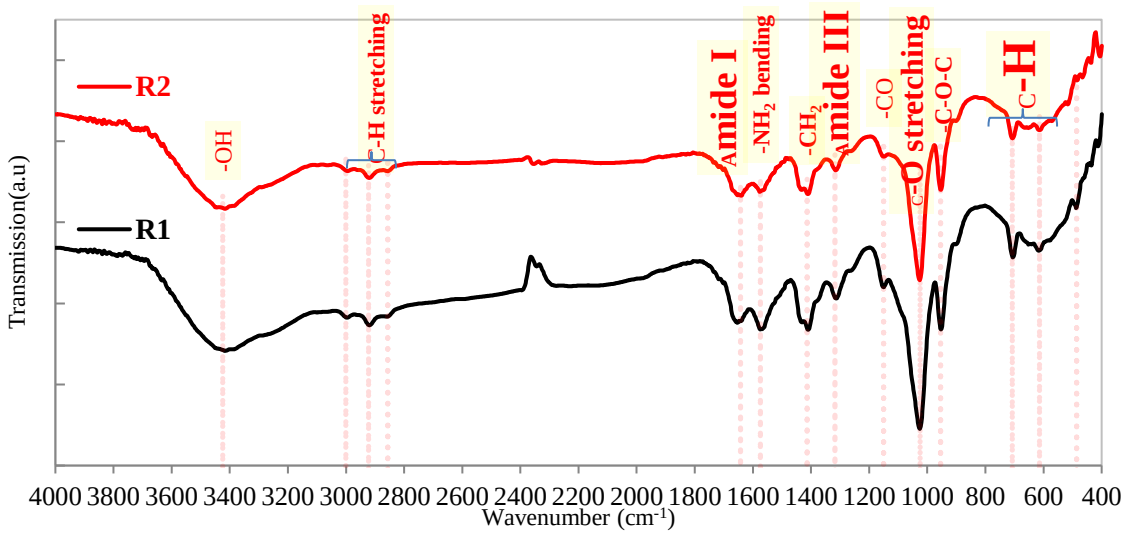

Figure 2: FTIR spectra of the Cs:PANI blend samples (R1 and R2).

Table 3: Primary FTIR absorption characteristics and assignments of R1 and R2.

Vibration Mode	R1 (cm^{-1})	R2 (cm^{-1})	Assignment / Description
O–H Stretching	3400	3402	Hydroxyl group vibrations in Cs
C–H Stretching	2850–2950	2850–2950	Aliphatic C–H vibrations
Amide I (C=O)	1654.96	1642.65	Carbonyl stretching of amide bond
NH_2 Bending	1568.83	1573.75	N–H bending, hydrogen bonding interactions
CH_2 Bending	1408.89	1413.81	C–H bending vibration
Amide III	1312.92	1317.84	C–N stretching coupled with N–H bending
C=O Stretching	1150.51	1150.51	Carbonyl stretching
C–O–C Stretching	953.66	953.66	Ether linkages
C–H Bending	616.54	614.08	Aromatic ring vibration
Low-Frequency Band	486.12	513.19	Structural deformation mode

3.2. UV-Visible Spectroscopy

Figs. 3 and 4 show the UV-Visible spectra of Cs:PANI blend films (R1 and R2), respectively. Both samples have extended absorption bands in the visible and ultraviolet regions, and this demonstrates that polyaniline has numerous electronic transitions linked to the conjugated π-system.

In sample R1, the absorption strength is not very strong in the visible range, but it rises drastically at around 900 nm, which is associated with the 900 nm π–π* transitions amongst the benzenoid rings within PANI. R2, in contrast, has stronger and extended absorption in the 700-800 nm range, a fact attributed to n- π* transitions associated with the quinoid structure. This implies that there is increased conjugation and delocalization of the electrons in R2 because of the improved distribution of PANI and increased strength of the molecular interactions in the film**.** Both samples have significantly extended absorption bands with higher absorption, which ensures multiple electronic transitions. The observed intense visible absorption suggests that the blends have a semiconducting nature as well as typical coloration due to their π-conjugated structure [15]. The Tauc approach, valid for amorphous and conjugated polymer systems, was used to evaluate the optical band gap (E_g) of the samples.

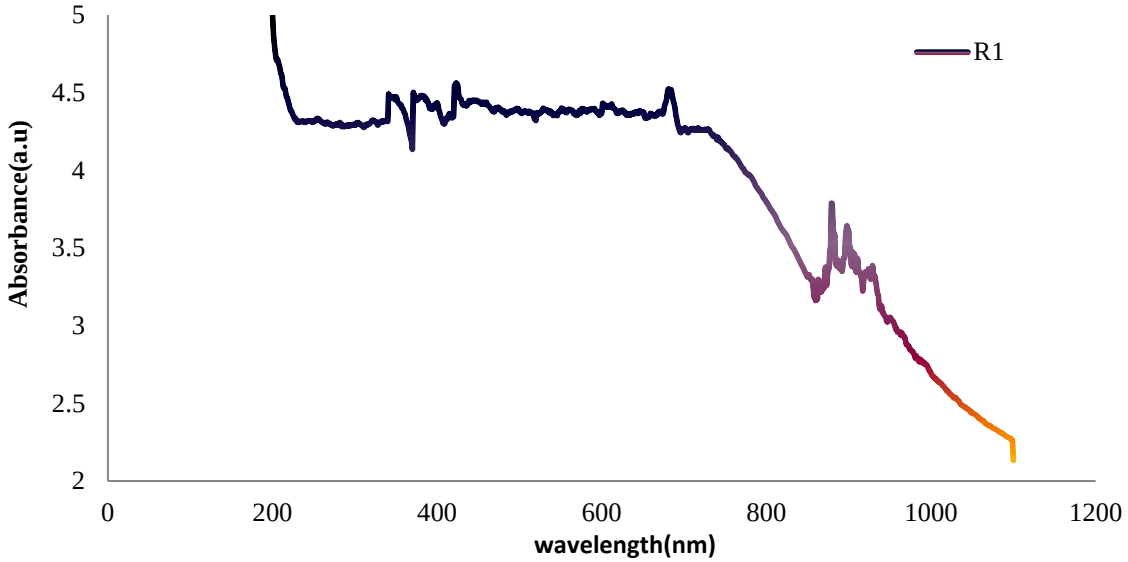

Figure 3: UV-visible spectra of sample R1 (Cs: PANI).

Fig. 4 represents the UV-visible absorption spectrum of the R2 blend samples as a function of wavelength. The absorbance generally increased with increasing wavelength, reaching its highest value near 900 nm. Several minor spectral features were also observed between approximately 200 and 750 nm, which may be associated with electronic transitions and variations in the conjugated structure of the Cs:PANI blend. The broad increase in absorption toward the near-infrared region may indicate enhanced electronic delocalization and stronger interactions between the polymer chains. However, assigning individual absorption features to specific electronic transitions requires additional spectroscopic evidence. The Tauc method can be used to determine the optical band gap of polymeric and hybrid materials, where the absorption edge is obtained directly from the wavelength at which the absorption increases sharply [16, 17]. Tauc plot is another method to determine the energy band gap (E_g). The plot is drawn according to Eq. (1) [18]:

$$\alpha h\nu = A\,(h\nu - Eg)^{n} \qquad (\mathbf{1})$$

where h is Planck's constant, ν is the photon's frequency, α is the absorption coefficient, n is an exponent determined by the nature of the electronic transition, and A is a proportionality constant [19].

Energy gap values for R1 and R2, determined from Tauc plots, are shown in Fig. 5 a and b and Table 4. The optical band gap values changed from 2.0 eV for R1 to 1.8 eV for R2, demonstrating that the reagent proportions used during PANI synthesis influenced the electronic structure of the blends. The lower band gap of R2 may facilitate charge transport; however, the present measurements alone do not establish a direct causal relationship between band-gap reduction and conductivity.

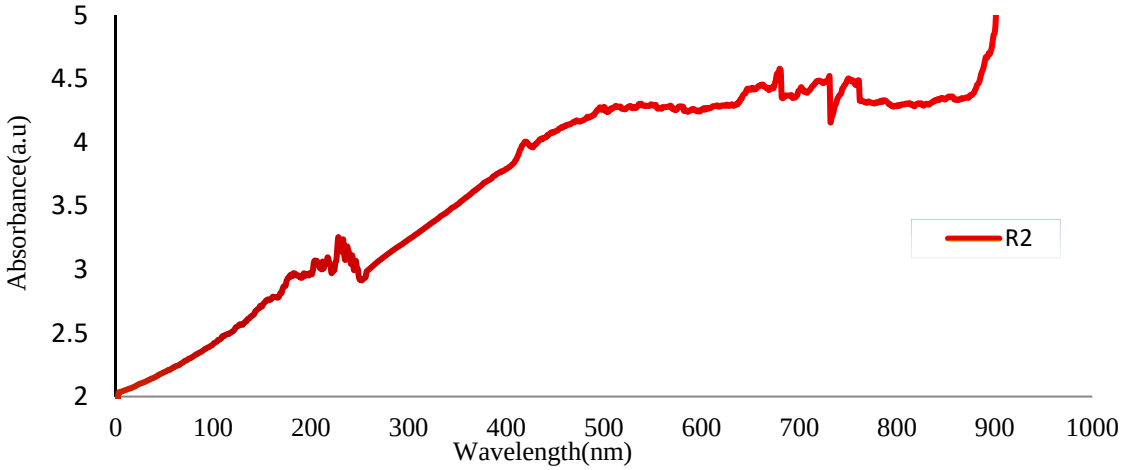

Figure 4: UV-visible spectra of blend sample R2 (Cs: PANI).

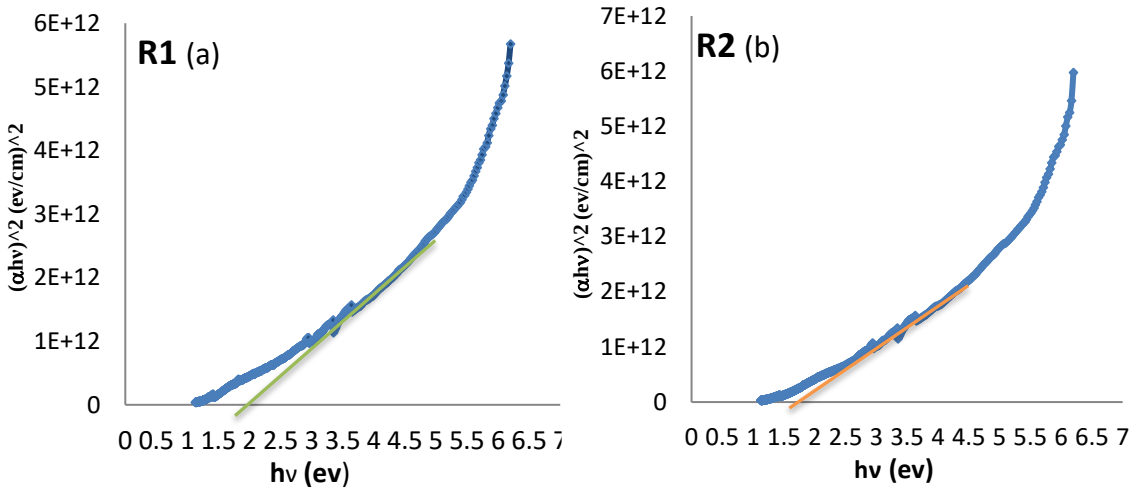

Figure 5: Tauc plots of $(\alpha h\nu)^2$ vs. photon energy (hν) for (a) R1and (b) R2.

Table 4: Optical band gap of R1 and R2.

Samples	λ onset (nm)	E_g (eV)
R1	700	2.0
R2	900	1.8

3.3. AC Conductivity

The electrical conductivity (σ) was calculated using Eq. (2):

$$\sigma = \frac{L}{R_b \times A} \quad (2)$$

where L is the thickness of the film =1.5 mm, R_b is the impedance of the sample, and A is the mean area of the electrodes = 1.77 cm² [20]. Fig. 6 illustrates the impedance behavior of the Cs:PANI blend samples (R1 and R2), and Table 5 summarizes the electrical conductivity values calculated for both samples. **S**ample R2 exhibited a lower bulk resistance (Z_r) value than R1. Because conductivity is inversely proportional to R_b, R2 showed higher electrical conductivity under the stated measurement conditions.

Using Eq. 2, the conductivities are 8.47×10^{-3} and 1.06×10^{-2} S cm^{-1}, respectively. The lower resistance and higher conductivity of R2 indicate improved charge transport, which may be associated with more effective PANI dispersion and contact between the two polymeric phases [21,22].

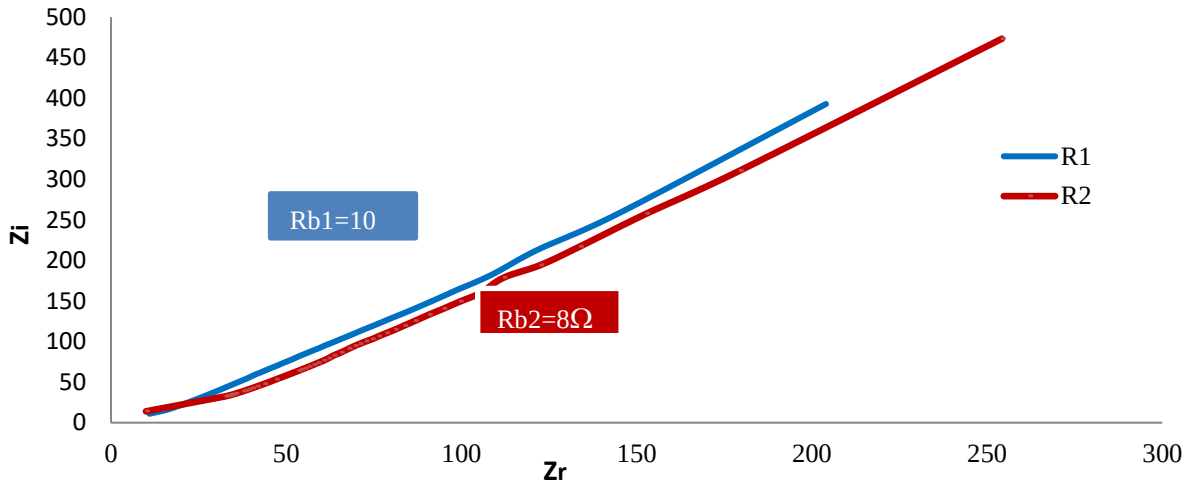

Figure 6: Relationship between resistance (Z_r) and impedance (Z_i) for (Cs: PANI) blend R1 and R2.

Table 5: Electrical conductivity of Cs:PANI blend samples (R1 and R2).

Sample	R_b (Ω)	Conductivity (S. cm^{-1})
R1	10	8.47×10^{-3}
R2	8	1.06×10^{-2}

3.4. Scanning Electron Microscope (SEM)

Fig. 7 (a and b) shows the scanning electron microscope (SEM) micrographs of the Cs:PANI blend samples R1 and R2 at 10,000× magnification. Sample R1 exhibited a heterogeneous and coarse surface morphology, with large, irregular agglomerates distributed throughout the matrix. In contrast, R2 showed smaller and more uniformly dispersed features, with apparent sizes ranging from 80 to 120 nm, compared with approximately 150-250 nm for R1. The finer and more homogeneous morphology of R2 may indicate improved PANI dispersion and enhanced interfacial interaction between Cs and PANI [23]. However, the bright and dark regions observed in the SEM micrographs cannot be conclusively assigned to specific phases without compositional analysis, such as energy-dispersive X-ray spectroscopy (EDS) mapping.

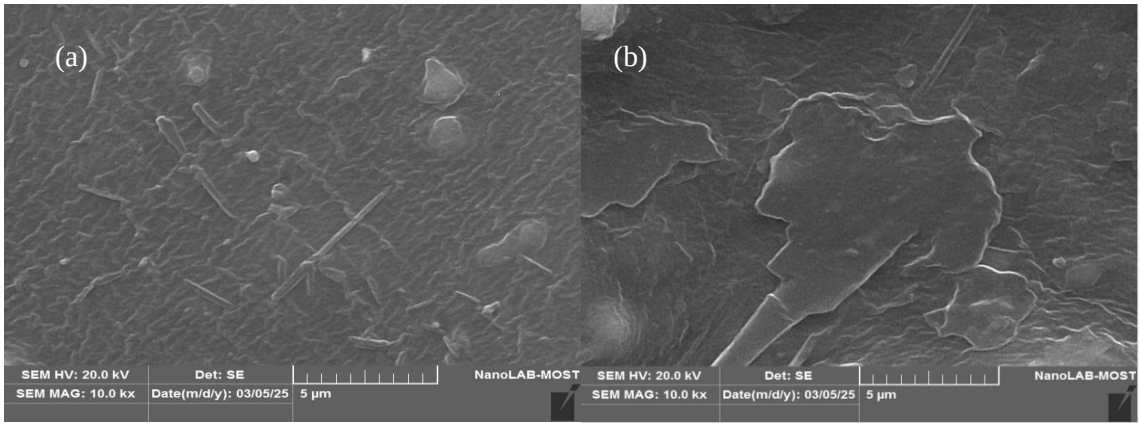

Figure 7: SEM images of Cs:PANI blends at 10k× magnification: (a) R1 and (b) R2.

3.5. Differential Scanning Calorimetry (DSC) Analysis

Differential Scanning Calorimetry (DSC) analysis was performed under a nitrogen (N_2) atmosphere to limit oxidation during analysis. The thermal parameters, such as the glass transition temperature (T_g), melting temperature (T_m), and decomposition temperature (T_d), were determined from duplicate thermograms with estimated uncertainties of 1-2 ^oC. Sample R1 (Fig. 8a) showed the first endothermic transition, T_g at about 101.65 °C, where chitosan chains relax and absorbed or weakly bound water is lost. The second change occurred at 168.8 ^oC, the T_m, which is probably related to the partial melting or the rearrangement of the PANI constituent. The third thermal event at 258.57 ^oC is an exothermic peak in the decomposition corresponding to T_d, an indicator of polymer degradation and potential crosslinking in the blend. Fig. 8b shows the thermal behavior of sample R2. Compared withR1, Sample R2 exhibited lower thermal transition temperatures, with T_g decreasing from 101.65 to 90.80 C and T_m decreasing from 168.80 to154.34 °C. These reductions may indicate increased polymer-chain mobility and decreased intermolecular constraints resulting from the higher oxidant-to-monomer ratio during PANI synthesis. In contrast, the decomposition temperature T_d increased from 258.57 °C for R1 to approximately 275.45 ^oC for R2, indicating improved thermal stability. This improvement may be associated with stronger interfacial interactions and structural arrangement within the cs: PANI [24].

Overall, R2 exhibited higher thermal stability and higher electrical conductivity than R1, together with lower T_g and T_m values. Table 6 represents a quantitative comparison of the two samples.

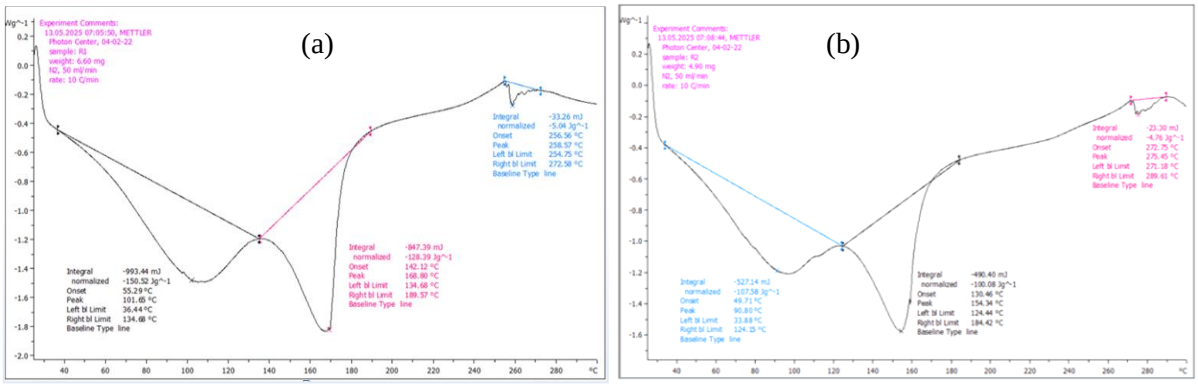

Figure 8: DSC analysis of Cs:PANI blends for (a) R1 and (b) R2.

Table 6: Quantitative comparison between R1 and R2.

Property	R1	R2
Band gap (E_g) eV	2.0	1.8
Electrical conductivity ($S.cm^{-1}$)	8.47×10^{-3}	1.06×10^{-2}
Glass transition temperature (T_g, °C)	101.65	90.8
Melting temperature (T_m, °C)	168.8	154.34
Decomposition temperature (T_d, °C)	258.57	275.45

4. Conclusions

Cs/PANI biopolymer electrolyte films were prepared by the solution casting method using PANI synthesized with different oxidant and monomer properties. The preparation conditions influenced the structural, optical, thermal, morphological, and electrical properties of the blends. FTIR and SEM analyses indicated intermolecular interactions and improved PANI dispersion in R2. Compared with R1, R2 exhibits a lower optical band gap, lower bulk resistance, higher calculated electrical conductivity, and higher decomposition temperature. These findings show that controlling the reagent proportions during PANI synthesis is an effective strategy for tuning the charge transport and thermal properties of Cs/PANI blends for potential flexible electronic and solid-state energy-related applications.

Acknowledgments

The authors would like to express their gratefulness towards the support of the research by the University of Baghdad/College of science/Department of Physics.

Conflict of Interest

The authors declare no conflicts of interest.

References

1. V. Cyriac, I. Ismayil, K. Mishra, A. Rao, S. P. Masti, and I. M. Noor, Compositional dependence of electrochemical properties in biopolymer blend-based solid electrolytes doped with sodium perchlorate for EDLC applications, *Electrochimica Acta* 507(10), 145139 (2024). https://doi.org/10.1016/j.electacta.2024.145139 .
2. S. Hadad, M. Hamrahjoo, H. Khezraqa, M. Golshan, Z. Wang, and M. S. Kalajahi, Starch acetate grafted to MXene composite surpasses room temperature liquid electrolyte performance for all-solid-state lithium-ion batteries. *Adv. Sci*. **12**(29), 1 (2025). https://doi.org/10.1002/advs.202503285.
3. M. Zhang, U. Pal, F. Makhlooghiazad, L. A. O'Dell, S. Kondou, G. A. Elia, C. Gerbaldi, and M. Forsyth, Advanced high-voltage electrolyte design using poly(ethylene oxide) and high-concentration ionic liquids for all-solid-state lithium-metal batteries. *ACS Appl. Mater. Interfaces*. **16**(41), 56095 (2024). https://doi.org/10.1021/acsami.4c11114.
4. R. Y. Mahmood, A. A. Kareem, Anji Reddy Polu and Sun Theo Constan Lotebulo Ndruru, Structural, electrical, and electrochemical investigations on Cu ion–conducting PVA/HPMC-based blend solid polymer electrolytes. *Ionics.* **30**(11), 7061 (2024). https://doi.org/10.1007/s11581-024-05822-9.
5. K. Sari, A. N. M. Haryadi, N. Khusaenah, S. E. Yulianti, and A. B. S. Utomo, Modification of chitosan/peg4000 dispersed with lithium triflate ($LiCF_3SO_3$) as a solid polymer electrolyte for the secondary battery. *Commun. Sci. Technol.* **9** (2), 243 (2024). https://doi.org/10.21924/cst.9.2.2024.1496.
6. H. R. Kttafah and H. S. Mahmood, Structural and mechanical properties of chitosan/PVA composite reinforced by Ag/Au. *in Proc. 3rd Annu. Int. Conf. Inf. Sci. (AICIS), Univ. of Fallujah, Iraq*, **18** Jun. (2024). https://dx.doi.org/10.57647/j.jtap.2024.si-AICIS23.06.

7. R. M. Hussein and F. A. Kareem, Synergistic antibacterial effect of chitosan/silver nanoparticles modified glass ionomer cement (an in vitro study), *Oxf. Open Mater. Sci.* **4**(1), 2024. https://doi.org/10.1093/oxfmat/itae013.
8. A. A. Mejrion, M. I. Isa, and M. Muthurivagaram, Structural studies of solid biopolymer electrolyte system based on 2-hydroxyethyl cellulose blend with ammonium chloride. *J. Adv. Res. Des.* **126(**1), 15 (2025). https://doi.org/10.37934/ard.126.1.1525.
9. A. M. Qusay and M. K. Jawad, Investigation of optical and electrical properties of solid polymer electrolyte based on natural polymer. *Iraqi J. Phys.*, **23**(3), 75 (2025). https://doi.org/10.30723/ijp.v23i3.1395.
10. T. S. Soliman, Effects of SiO_2 nanoparticles on polyvinyl alcohol/carboxymethyl cellulose polymer blend films' structural, wettability, surface roughness, and optical characteristics. *Adv. Polym. Technol.* **2024** (1), 3623198 (2024). https://doi.org/10.1155/2024/3623198.
11. F. M. Ahmed and M. K. Jawad, Nanocomposites electrolytes based conductive polymer for electrochemical application. *J. Theor. Appl. Phys., Special Issue AICIS'23*, Article 23, Jun. (2024). https://dx.doi.org/10.57647/j.jtap.2024.si-AICIS23.23.
12. K. M. Manikandan, A. Yelilarasi, S. S. Saravanakumar, P. Senthamaraikannan, A. Khan, and A. M. Asiri, Effect of imidazole based polymer blend electrolytes for dye-sensitized solar cells in energy harvesting window glass applications. *Chin. J. Chem. Eng.* **27**(11), 2807 (2019). https://doi.org/10.1016/j.cjche.2019.03.034.
13. M. Teodorescu, M. Bercea, and S. Morariu, Biomaterials of PVA and PVP in medical and pharmaceutical applications: Perspectives and challenges. *Biotechnol. Adv.* **37**(1), 109 (2019). https://doi.org/10.1016/j.biotechadv.2018.11.008.
14. J. Li, K-D Wu, H. Shan, J-H Zhang, M. Zhao, G-B Gong, W-L Guo and Y-B Wu, Synthesis and properties of hydroxytelechelic polyisobutylenes by end capping with *tert*-Butyl-dimethyl-(4-methyl-pent-4-enyloxy)-silane. *Chin. J. Polym. Sci.* **37** (9), 936 (2019). https://doi.org/10.1007/s10118-019-2327-8.
15. M. Andonegi, K. L. Heras, E. Santos-Vizcaino, R. M. Igartua, R. M. Hernandez, K. de la Caba, and P. Guerrero, Structure-properties relationship of chitosan/collagen films with potential for biomedical applications. *Carbohydr. Polym.* **237**, 116159 (2020). https://doi.org/10.1016/j.carbpol.2020.116159.
16. C. Rodrigues, D. M. J. Irfan, J. Lahanandran, D. J. Macuvele, J. Padoin, N. Kipper, M. L. M. Teske, and N. Teske, Mechanical, thermal and antimicrobial properties of chitosan-based-nanocomposite with potential applications for food packaging. *J. Poly. Environ.* **28**(9), 1216 (2020). https://doi.org/10.1007/s10924-020-01678-y.
17. R. K. Shamki and A. A. Hasan, Analysis of the electrical and optical properties of polyaniline/graphene oxide/metal oxides nanocomposites. *Iraqi J. Phys.* **23**(4), 53(2025). https://doi.org/10.30723/ijp.v23i4.1434.
18. M. Rinaldo, Chitin and chitosan: properties and applications, *Prog. Polym. Sci.* **31**(7), 603 (2006). https://doi.org/10.1016/j.progpolymsci.2006.06.001.
19. A. A. Essawy, M. F. Hussein, T. H. A. Hasanin, E. F. El Agammy, H. S. Alsaykhan, R. F. Alanazyi, and A. El Essawy, Insights for precursors influence on the solar-assisted photocatalysis of greenly synthesizing zinc oxide NPs towards fast and durable wastewater detoxification. *Ceramics*. **7**(3), 1100 (2024). https://doi.org/10.3390/ceramics7030072.
20. M. K. Jawad, F. T. M. Noori, A. N. Ali, S. I. Hussein, A. A. Kareem, and A. R. Paul, Preparation and characterization of PVA/MWCNT nanocomposites: a composition dependence study of structural, optical and mechanical properties. *Fullerenes, Nanotubes and Carbon Nanostructures*, **33**(1), 50 (2025).https://doi.org/10.1080/1536383X.2024.2387146.
21. N. Gewili, A. M. Abdelghany, M. Mekhaimer and A. Oraby, Synthesis and optical properties of chitosan/polypyrrole composite for biological applications. *Lett. Appl. NanoBioScience*. **10**(4), 2742 (2021). https://doi.org/10.33263/LIANBS104.27422749.
22. J. Huang and R. B. Kaner, A General Chemical Route to Polyaniline Nanofibers. *J. Amer. Chem. Soc.* **126** (3), 851 (2004). https://doi.org/10.1021/ja0371754.
23. H. Ohno, *Electrochemical aspects of ionic liquids*, Wiley & Sons, Inc., (2005). https://doi.org/10.1002/0471762512.
24. M. J. John and S. Thomas, Biofibres and Biocomposites. *Carbohydr. Polym.* **71**(3), 343 (2008). http://dx.doi.org/10.1016/j.carbpol.2007.05.040.

تأثير نسبة المؤكسد على السلوك البنيوي والكهربائي للإلكتروليت الحيوي القائم على مزيج البولي أنيلين - الكيتوسان

ايلاف علي سوادي[1] و محمد كاظم جواد[1]
[1] قسم الفيزياء، كلية العلوم، جامعة بغداد، بغداد، العراق

الخلاصة
تم تحضير أغشية إلكتروليتية من البوليمر الحيوي الكيتوزان/بولي أنيلين (Cs/PANI) باستخدام طريقة صب المحلول لدراسة تأثير نسبة المؤكسد إلى المونومر أثناء تصنيع البولي أنيلين على خصائصها البنيوية والبصرية والحرارية والمورفولوجية والكهربائية. أكد التحليل الطيفي بالأشعة تحت الحمراء بتحويل فورييه (FTIR) التفاعل بين الكيتوزان والبولي أنيلين من خلال انزياحات مميزة في نطاقات الامتصاص، مما يشير إلى تعزيز التفاعلات بين الجزيئات. وكشف تحليل الأشعة فوق البنفسجية والمرئية أن زيادة نسبة المؤكسد قللت فجوة النطاق البصري من 2 إلى 1.8 إلكترون فولت، بينما أظهرت القياسات الكهربائية تحسنًا في التوصيلية الكهربائية من 8.47×10^{-3} و 1.06×10^{-2} سيمنز/سم. وكشف المجهر الإلكتروني الماسح (SEM) عن توزيع أكثر تجانسًا للبولي أنيلين داخل مصفوفة الكيتوزان، مع انخفاض تكتل الجسيمات. في المقابل، أشار التحليل الحراري التفاضلي الماسح (DSC) إلى تحسن الاستقرار الحراري وزيادة حركة سلسلة البوليمر. تُظهر هذه النتائج أن تحسين نسبة المؤكسد هو نهج فعال لتعزيز التنظيم الهيكلي ونقل الشحنة والأداء الحراري لإلكتروليتات البوليمر الحيوي Cs/PANI، مما يسلط الضوء على إمكاناتها لتخزين الطاقة في الحالة الصلبة والتطبيقات الإلكترونية المرنة.

الكلمات المفتاحية: البولي أنيلين، الكيتوزان، البلمرة التأكسدية، الخصائص الفيزيائية، التوصيل الأيوني.